Optical Second Harmonic Generation of Single Metallic Nanoparticles Embedded in a Homogeneous Medium

ARTICLE *in* NANO LETTERS · MAY 2010

Impact Factor: 13.59 · DOI: 10.1021/nl1000949 · Source: PubMed

7 AUTHORS, INCLUDING:

Jérémy Butet
École Polytechnique Fédérale de Lausanne
28 PUBLICATIONS **421** CITATIONS
SEE PROFILE

Emmanuel Benichou
Claude Bernard University Lyon 1
92 PUBLICATIONS **1,656** CITATIONS
SEE PROFILE

Christian Jonin
Claude Bernard University Lyon 1
82 PUBLICATIONS **1,246** CITATIONS
SEE PROFILE

Pierre-Francois Brevet
Claude Bernard University Lyon 1
173 PUBLICATIONS **2,861** CITATIONS
SEE PROFILE

NANO LETTERS

pubs.acs.org/NanoLett

Optical Second Harmonic Generation of Single Metallic Nanoparticles Embedded in a Homogeneous Medium

Jérémy Butet, Julien Duboisset, Guillaume Bachelier,* Isabelle Russier-Antoine, Emmanuel Benichou, Christian Jonin, and Pierre-François Brevet

Laboratoire de Spectrométrie Ionique et Moléculaire, Université Claude Bernard Lyon 1 - CNRS, UMR 5579, 43 Boulevard du 11 Novembre 1918, 69622 Villleurbanne, France

ABSTRACT We report the optical second harmonic generation from individual 150 nm diameter gold nanoparticles dispersed in gelatin. The quadratic hyperpolarizability of the particles is determined and the input polarization dependence of the second harmonic intensity obtained. These results are found in excellent agreement with ensemble measurements and finite element simulations. These results open up new perspectives for the investigation of the nonlinear optical properties of noble metal nanoparticles.

KEYWORDS Single nanoparticle, gold, plasmonics, nonlinear optics, second harmonic generation, finite element method simulation

The observation of single objects the dimensions of which are much smaller than the wavelength of light has become a great technical challenge in optical sciences. The detection of single molecules has already been achieved with light emission-based techniques like fluorescence or Raman scattering.[1,2] Single metallic particle sensitivity has also been demonstrated in the past and applied to the investigation of the linear optical properties of metallic nanoparticles, and their absorption cross-section in particular, overcoming the heterogeneous broadening inherent to shape and size distributions of real samples.[3] Combined with numerical simulations, the size, shape, and orientation of single nanostructures such as metallic nanorods can be precisely determined although their size is largely below the diffraction limit.[4] Correlating the optical properties with that obtained from transmission electronic microscopy further deepens the understanding of the link between morphology and linear optical properties. This is especially true for coupled particles when the interparticle distance or the radius of curvature of the particle surface approaches the electron spill-out thickness.[5]

Nonlinear optical techniques, and more precisely second harmonic (SH) generation, the phenomenon whereby two photons at the fundamental frequency are converted into one photon at the harmonic frequency, have also been widely used for the investigation of noble metal particles produced by wet chemical synthesis and dispersed in solutions[6−11] or metallic nanostructures produced by e-beam lithography methods on substrates for instance.[12−15] However, only few works have been devoted to single particle analyses.[16−19] This is mainly due to the very weak signals expected for second order nonlinear optical processes like SH generation. These second order processes are indeed forbidden within the electric dipole approximation in centrosymmetric materials such as silver and gold. Furthermore, in small particles with a centrosymmetric shape, where small must be understood as much smaller than the wavelength of light, these second order processes allowed at the particle surface where the centrosymmetry of the material is broken vanish also for the same symmetry reasons. As a result, any deviation from centrosymmetry yields a nonvanishing SH intensity. For small particles, the SH response is thus dominated by the electric dipole contribution arising from the shape centrosymmetry breaking if the material centrosymmetry is assumed preserved.[8,20] In ensemble measurements, the averaging over the size, shape, and orientation distributions prevents one from getting a deeper understanding on the origin of the nonlinear optical properties of metal nanoparticles. With the availability of the required sensitivity,[21] going to the single particle level appears as a promising tool to go beyond ensemble measurements and investigate single metallic particles with a technique sensitive to shape centrosymmetry breaking.

In this letter, we report for the first time experiments where the SH intensity of a single metallic nanoparticle dispersed in a homogeneous medium is achieved. The quadratic hyperpolarizability determined is compared with standard hyper Rayleigh scattering (HRS) measurements on ensemble solutions[8] and with previous experiments where single metallic nanoparticle sensitivity was achieved with HRS measurements with low-concentration solutions.[21] In addition, the homogeneous and isotropic environment of the

* To whom correspondence should be addressed. E-mail: guillaume.bachelier@lasim.univ-lyon1.fr.

Received for review: 01/12/2010
Published on Web: 04/26/2010

DOI: 10.1021/nl1000949 | *Nano Lett.* **2010,** *10,* 1717–1721

nanoparticle used in the present configuration allows a direct comparison with theoretical simulations obtained with finite element method (FEM).[20] In particular, the SH intensity polarization pattern of a single gold metallic nanoparticle is used to further ensure that a single particle is observed and assess the nature of the SH fields in terms of the multipolar plasmon excitations.

The experimental setup was designed as follows. A mode-locked Ti:sapphire laser tuned to a wavelength of 794 nm and delivering pulses of about 180 fs at a repetition rate of 76 MHz was used as the laser source. The average output power was set at about 300 mW right after the laser exit. The fundamental beam was focused into a quartz cell with a microscope objective (×16, NA 0.32) and a red filter was placed in front of it to remove any residual light at the harmonic frequency generated prior to the cell. The cell position with respect to the laser focus was controlled by three micrometer-resolution translation stages (Newport, MFA-CC). The SH intensity collection was performed at right angle with a 25 mm focal length lens with a numerical aperture of 0.5. A blue filter was placed before a monochromator to remove the fundamental light. The detection was made with a cooled photomultiplier tube and the fundamental beam was chopped at 130 Hz to enable a gated photon counting regime allowing the removal of the background photons. The sketch of the setup can be found in ref 22. The aqueous solutions of the gold nanoparticles, the average diameter of which was about 150 nm, were purchased from BBI International and used as received. The gold nanoparticles were dispersed in a gelatin matrix (BLOOM 250, 8%). The gelatin matrix was obtained by raising the temperature of a water−gelatin mixture beyond the critical temperature at about 70 °C for 20 min and then cooled down to 4 °C for 12 h in the quartz cell with the particles. Gelatin is transparent at the wavelengths of excitation at 794 nm and SH emission at 397 nm and possesses a weak SH efficiency as required in order not to dwarf the SH signals from the gold nanoparticles.

The sample scans were carried out perpendicularly to the incident fundamental beam direction in order to obtained two-dimensional (2D) maps of the SH intensity versus cell position; see Figure 1. The heterogeneous spatial distribution of the SH intensity reveals areas with low (Zone 1) and high (Zone 2) intensities. The SH intensity from Zone 1 corresponds to the signal recorded for neat gelatin, that is, without particles, indicating that the low-intensity areas are composed exclusively of gelatin. In Zone 2 however, the SH intensity is significantly increased. This is attributed to the presence of the gold metal nanoparticles in this zone. To reject the possibility of other origins like gelatin inhomogeneities, broadband emission spectra of Zones 1 and 2 were recorded; see Figure 2. Two distinct features are observed, a narrow peak at 397 nm corresponding to the SH intensity and the onset of a broadband background with an increasing intensity toward longer wavelengths attributed to the gelatin

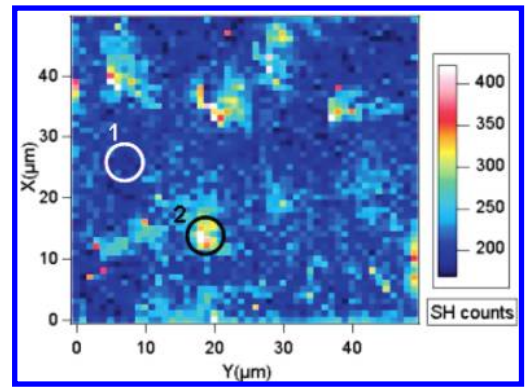

FIGURE 1. Two dimensional map of the SH intensity at 397 nm obtained for 150 nm gold nanoparticles embedded in gelatin by scanning the sample perpendicularly to the beam direction with 10s acquisition time per pixel. The two circles correspond to Zone 1 and Zone 2 as discussed in the text.

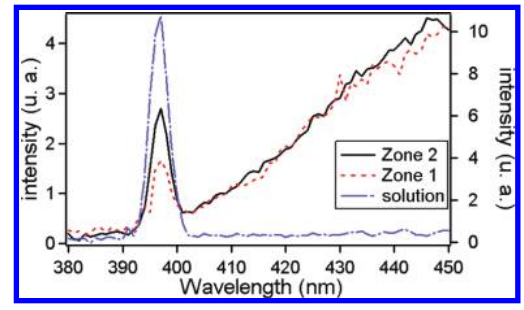

FIGURE 2. Emission spectrum from the zones 1 and 2 shown in Figure 1 for an excitation at 794 nm and 80 s acquisition time for each data point (left axis) and emission spectrum of 150 nm gold nanoparticles in solution (right axis).

multiphoton excited luminescence. This broadband luminescence background is identical in the two Zones 1 and 2 to that obtained from a neat gelatin sample without particles. Gelatin inhomogeneities are therefore not responsible for the large intensity recorded in Zone 2. One therefore concludes that the high intensity areas are related to the presence of the gold metal nanoparticles. This conclusion is further supported by the broadband emission spectrum obtained for an aqueous solution of these gold metallic nanoparticles, where almost no photoluminescence is observed.

The nonlinear efficiency of the gold metallic nanoparticles can be obtained by subtracting the SH intensity of the neat gelatin area, Zone 1, from the high intensity one, Zone 2; see Figure 2. The gelatin matrix can be used as an internal reference to determine the quadratic hyperpolarizability of the 150 nm diameter gold nanoparticles. For this purpose, the SH intensity scattered from a neat water cell and obtained under the same experimental conditions was used as an external reference for the neat gelatin. The refractive index of the gelatin, estimated either form a simple averaged value based on the water/gelatin molar ratio or from the shift of the surface plasmon resonance wavelength of the gold particles dispersed in water with respect to the resonance wavelength of those dispersed in gelatin, was found to be

DOI: 10.1021/nl1000949 | *Nano Lett.* **2010,** *10,* 1717–1721

1.36 as compared to 1.33 for pure water. This allows the neglect of any changes in the reflection conditions at the cell surface and any modification of the beam waist size and position in the cell. The SH intensities obtained for neat water and neat gelatin can hence be directly compared. The SH intensity of neat gelatin was found to be 2.5 times larger than that of neat water. The intensity radiated at the harmonic frequency for gelatin in the presence of the metallic particles can therefore be written as

$$I_{SHG} = G \int (2.5 C_w \langle \beta_w^2 \rangle I_\omega^2 + \beta_{part}^2 I_{\omega,part}^2) dV \qquad (1)$$

where C_w and $\beta_w = 0.56 \times 10^{-30}$ esu[23] are the concentration and quadratic hyperpolarizability of water, respectively. β_{part} stands for the quadratic hyperpolarizability of a single gold nanoparticle and $I_{\omega,part}$ for the fundamental intensity of the fundamental beam illuminating the gold nanoparticle. Note that the response of the particles and that of the gelatin background have been summed up incoherently in eq 1. This is allowed owing to the random orientations and positions of the gelatin molecules across the laser beam, leading to an intrinsically incoherent response as observed Hyper Rayleigh Scattering.[24] There is therefore no interference between the particle and the background responses.

There are two major difficulties in eq 1. (i) One has to determine properly the integral $\int I_\omega^2 \, dV$ of the squared fundamental intensity over the focused beam to determine the gelatin internal reference and (ii) one has to know precisely where the gold nanoparticle is located with respect to the fundamental beam waist. These two difficulties must be overcome simultaneously in order to take into account the fact that the gold particle, because of its small size, does not probe to whole cross-section of the fundamental beam but rather only a small portion of it. To address the first difficulty (i), 2D maps were recorded for 300 nm diameter fluorescein-doped latex particles. With the input fundamental beam wavelength fixed at 794 nm, these particles exhibit a strong two photon-excited luminescence leading to the same squared dependence of the fluorescence intensity with the fundamental beam intensity. The spatial autocorrelation of the 2D fluorescence maps were compared with simple calculations taking into account a random distribution of the fluorescent particles and a Gaussian beam with various waist sizes w_0. The best agreement was found for a beam waist of $w_0 \approx 5$ μm. Using this value as an input parameter, the integral $\int I_\omega^2 \, dV$ was easily computed. The second difficulty (ii) is more difficult to handle since the present method cannot determine the exact position of the gold particle along the beam propagation direction. A simple scan of the sample along to the fundamental beam direction could be used to determine that the particle position in this direction. However, the Rayleigh length $l = \pi w_0^2/\lambda = 140$ μm associated with the fundamental Gaussian beam is too long to perform this experiment without misalignment of the focus. Instead, 2D SH maps in different locations in the sample were recorded and from the highest intensity, corresponding to positions of the particle in the or very close to the beam waist, a quadratic hyperpolarizability $\beta_{part} = (1.0 \pm 0.15) \times 10^{-23}$ esu was measured. This value is in excellent agreement with ensemble measurements where a value of $\langle \beta_{part} \rangle = (1.1 \pm 0.1) \times 10^{-23}$ esu was obtained.[8] In the latter case, the brackets stand for the size, shape, and orientational average owing to the ensemble nature of the measurement.

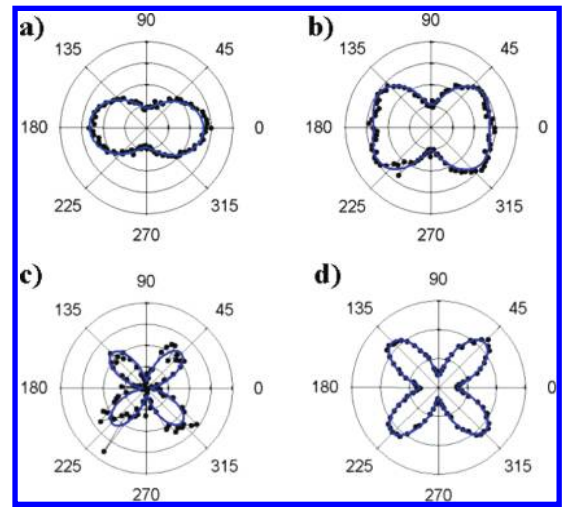

FIGURE 3. Vertically polarized SH intensity from Zone 1 (a) and Zone 2 (b) shown in Figure 1 with 80 s acquisition time for each data point. The corresponding difference is reported in panel c. For comparison, the corresponding ensemble measurement is shown in panel d. All curves are fitted using the expression of the SH intensity given in the text.

In order to obtain a deeper understanding of the nonlinear optical nature of the signals collected at the single nanoparticle level and confirming that a single particle is observed, the SH intensities of the vertically polarized harmonic field from Zones 1 and 2 were measured as a function of the input polarization angle of the fundamental beam. In this case, a zero angle corresponds to the vertical polarization. As shown in Figure 3a, the SH intensity from Zone 1 exhibits a typical two lobes pattern due to the purely dipolar contribution from the gelatin matrix. The orientation and position of the gelatin and water molecules being random, their response adds up incoherently as it is the case in Hyper Rayleigh Scattering.[24] The obtained pattern corresponds therefore to that of an orientation averaged response of single gelatin and water molecules. The same measurement in Zone 2 shows a clear deviation from the pure dipolar response. As for the unpolarized measurements presented above, this additional contribution can be attributed to the gold metallic nanoparticle. Polar plots are usually fitted with the following expression[6–8]

$$I_{SHG}^V = a^V \cos^4 \gamma + b^V \cos^2 \gamma \sin^2 \gamma + c^V \sin^4 \gamma \qquad (2)$$

DOI: 10.1021/nl1000949 | *Nano Lett.* **2010,** *10,* 1717–1721

where the parameters a^V, b^V and c^V are related to the elements of the quadratic hyperpolarizability tensor. Besides, these coefficients obey specific relationships depending on the contribution they describe. For a pure electric dipolar response they are related through $a^V + c^V = b^V$ whereas for a pure electric quadrupole contribution, they are related through $a^V = b^V = 0$.[6] To quantify the ratio between these two dipolar and quadrupolar contributions, an empirical weighting parameter has been introduced in the past as[7]

$$\zeta^V = \left| \frac{b^V - (a^V + c^V)}{b^V} \right| \quad (3)$$

ζ^V ranges from zero for a pure dipolar response to unity for a pure quadrupolar one. As expected, experimentally, ζ^V is equal to 0.019 ± 0.002 in Zone 1 but rises to 0.37 ± 0.03 in Zone 2. The difference between the two polar plots mentioned above is therefore attributed to a quadrupolar contribution associated to the gold metallic nanoparticle presence. The neat signal from the nanoparticle can be obtained by subtracting the neat gelatin signal of Zone 1, see Figure 3a, from that recorded in Zone 2 and displayed in Figure 3c. One clearly recovers an almost pure quadrupolar response since the SH intensities obtained at angles 0 and $\pi/2$ almost completely vanish.[25] Despite the low signal-to-noise ratio of the single particle measurement, there is a clear difference from ensemble measurements. Indeed, as shown in Figure 3d, the ensemble measurements lead to non vanishing intensities at angles 0 and $\pi/2$ of the incident polarization in contrast to the single particle case, see Figure 3c. Furthermore, it has been reported in the past that elongated rodlike gold metallic particles are extremely sensitive to the angle between the particle long axis and the direction of the linear polarization of the exciting field.[26] Hence, the relatively equal SH intensities recorded at angles $\pi/4$, $3\pi/4$, $5\pi/4$, and $7\pi/4$, see Figure 3c, indicate that a single nanoparticle is observed and not a small aggregate of particles, like a dimer or trimer system, which would exhibit unequal SH intensities for these four angles of polarization. In this analysis, we do not consider the configuration where the long axis of a dimer aggregate would be perfectly aligned along the beam direction of propagation because of the extremely unfavorable probability of appearance of this configuration. Moreover, in this singular configuration, the responses of the two particles have to be summed up coherently. Therefore, neglecting further enhancement arising from near-field coupling, a four times larger SHG intensity is expected. Using the hyperpolarizability obtained from ensemble measurements, the spots would reach roughly 1000 SHG counts (200 SHG counts from the gelatin and 4×200 SHG counts from the dimer). Such a strong signal has never been observed in the cartographies performed in different locations in the sample and for different particle concentrations. This clearly demonstrates that the hypothesis of aggregates formation can be ruled out in the present experiments.

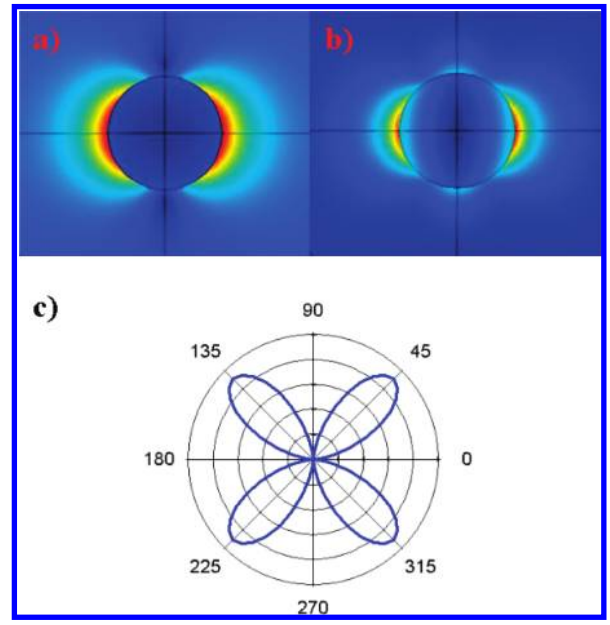

FIGURE 4. Near-field distribution of (a) the fundamental and (b) the harmonic fields for a 150 nm gold nanoparticle excited at a wavelength 794 nm. The corresponding far-field intensity collected at right angle for a vertical polarization is plotted as a function of the input polarization angle (c).

Finally, FEM simulations were also performed following the lines of that reported in ref 20. In the present simulations, a perfect spherical shape is assumed for the gold nanoparticle. The fundamental input field is first computed allowing for the calculation of the nonlinear sources; see Figure 4a. The harmonic field is then obtained by solving the Maxwell equations with the use of the weak form; see Figure 4b.[20] In a third step, the far-field scattered intensity is computed from the near-field distribution of the harmonic field. The result is shown in Figure 4c for a vertically polarized detection of the SH field. This polar graph is independent of the nonlinear sources assumed for the calculation, whether a surface or a bulk contribution for the nonlinear polarization. The agreement with the single particle experiment is excellent. Hence, it is concluded that the differences observed between single particle and ensemble measurements stem from the averaging procedure over different particle shapes leading to, in the case of strong deviations from the perfect spherical shape, the nonvanishing of the dipolar response owing to the breaking of the centrosymmetry.[20] The almost purely quadrupolar origin shown in Figure 3c provides evidence that the particle investigated has a near spherical shape, that is, the shape symmetry is not much broken. This result underlines the interest for performing single particle measurements as opposed to ensemble ones to allow for a direct comparison between experiments and simulations.

In conclusion, we have observed for the first time the SH intensity signal from a single metallic nanoparticle embed-

DOI: 10.1021/nl1000949 | *Nano Lett.* **2010,** *10,* 1717–1721

ded in a homogeneous medium. This configuration is critical to investigate the intrinsic nonlinear optical properties of nanoparticles without centrosymmetry breaking induced by the surrounding medium like for the configurations where the particles are supported on a substrate for example. The quadratic hyperpolarizability values obtained are in excellent agreement with ensemble measurements. Polarization resolved experiments have also been performed and compared to FEM simulations. The weak differences between single particle and ensemble measurements are attributed to the averaging of the SH response from particles with different size, shape and orientation in ensemble measurements. The achievement of single particle experiments and their direct comparison with FEM calculations open up new perspectives in the investigation of the nonlinear optical properties of metallic nanoparticles.

REFERENCES AND NOTES

(1) Mertz, J.; Xu, C.; Webb, W. W. *Opt. Lett.* **1995**, *20*, 2532.
(2) Kneipp, K.; Wang, Y.; Kneipp, H.; Perelman, L. T.; Itzkan, I.; Dasari, R. R.; Feld, M. S. *Phys. Rev. Lett.* **1997**, *78*, 1667.
(3) Muskens, O. L.; Del Fatti, N.; Vallée, F.; Huntzinger, J. R.; Billaud, P.; Broyer, M. *Appl. Phys. Lett.* **2006**, *88*, 063109–3.
(4) Muskens, O. L.; Bachelier, G.; Del Fatti, N.; Vallée, F.; Brioude, A.; Jiang, X.; Pileni, M. P. *J. Phys. Chem. C* **2008**, *112*, 8917.
(5) Marhaba, S.; Bachelier, G.; Bonnet, C.; Broyer, M.; Cottancin, E.; Grillet, N.; Lermé, J.; Vialle, J.-L.; Pellarin, M. *J. Phys. Chem. C* **2009**, *113*, 4349.
(6) Nappa, J.; Revillod, G.; Russier-Antoine, I.; Benichou, E.; Jonin, C.; Brevet, P. F. *Phys. Rev. B* **2005**, *71*, 165407.
(7) Nappa, J.; Russier-Antoine, I.; Benichou, E.; Jonin, C.; Brevet, P. F. *J. Chem. Phys.* **2006**, *125*, 184712.
(8) Russier-Antoine, I.; Benichou, E.; Bachelier, G.; Jonin, C.; Brevet, P. F. *J. Phys. Chem. C* **2007**, *111*, 9044.
(9) Chandra, M.; Indi, S. S.; Das, P. K. *Chem. Phys. Lett.* **2006**, *422*, 262.
(10) Chandra, M.; Das, P. K. *Chem. Phys. Lett.* **2009**, *476*, 62.
(11) Chandra, M.; Das, P. K. *Chem. Phys.* **2009**, *358*, 203.
(12) Canfield, B. K.; Kujala, S.; Jefimovs, K.; Turunen, J.; Kauranen, M. *Opt. Exp.* **2004**, *12*, 5418.
(13) Canfield, B. K.; Husu, H.; Laukkanen, B.; Bai, F.; Kuittinen, M.; Turunen, J.; Kauranen, M. *Nano Lett.* **2007**, *7*, 1251.
(14) Kujala, S.; Canfield, B. K.; Kauranen, M.; Svirko, Y.; Turunen, J. *Phys. Rev. Lett.* **2007**, *98*, 167403.
(15) Kujala, S.; Canfield, B. K.; Kauranen, M.; Svirko, Y.; Turunen, J. *Opt. Exp.* **2008**, *16*, 17196.
(16) Jin, R.; Jureller, J. E.; Kim, H. Y.; Scherer, N. F. *J. Am. Chem. Soc.* **2005**, *127*, 12482.
(17) Zavelani-Rossi, M.; Celebrano, M.; Biagioni, P.; Polli, D.; Finazzi, M.; Duo, L.; Cerullo, G.; Labardi, M.; Allegrini, M.; Grand, J.; Adam, P. M. *Appl. Phys. Lett.* **2008**, *92*, 093119.
(18) Lippitz, M.; van Dijk, M. A.; Orrit, M. *Nano Lett.* **2005**, *5*, 799.
(19) Canfield, B. K.; Husu, H.; Kontio, J.; Viheriälä, J.; Rytkönen, T.; Niemi, T.; Chandler, E.; Hrin, A.; Squier, J. A.; Kauranen, M. *New J. Phys.* **2008**, *10*, No. 013001.
(20) Bachelier, G.; Russier-Antoine, I.; Benichou, E.; Jonin, C.; Brevet, P. F. *J. Opt. Soc. Am. B* **2008**, *25*, 955.
(21) Duboisset, J.; Russier-Antoine, I.; Benichou, E.; Bachelier, G.; Jonin, C.; Brevet, P. F. *J. Phys. Chem. C* **2009**, *113*, 13477.
(22) Deniset-Besseau, A.; Duboisset, J.; Benichou, E.; Hache, F.; Brevet, P. F.; Schanne-Klein, M. C. *J. Phys. Chem. B* **2009**, *113*, 13437.
(23) Vance, F. W.; Lemon, B. I.; Hupp, J. T. *J. Phys. Chem. B* **1998**, *102*, 10091.
(24) Clays, K.; Persoons, A. *Phys. Rev. Lett.* **1991**, *66*, 2980.
(25) Dadap, J. I.; Shan, J.; Eisenthal, K. B.; Heinz, T. F. *Phys. Rev. Lett.* **1999**, *83*, 4045.
(26) Hubert, C.; Billot, L.; Adam, P.-M.; Bachelot, R.; Royer, P.; Grand, J.; Gindre, D.; Dorkenoo, K. D.; Fort, A. *Appl. Phys. Lett.* **2007**, *90*, 181105.

DOI: 10.1021/nl1000949 | *Nano Lett.* **2010,** *10,* 1717–1721